

Clustering of quasars in the First Year of the SDSS-IV eBOSS survey: Interpretation and halo occupation distribution

Sergio A. Rodríguez-Torres^{1,2,3*}, Johan Comparat^{1,3†}, Francisco Prada^{1,2,4},
Gustavo Yepes³, Etienne Burtin⁵, Pauline Zarrouk⁵, Pierre Laurent⁵, ChangHoon Hahn⁶,
Peter Behroozi⁷, Anatoly Klypin^{8,9}, Ashley Ross^{10,11}, Rita Tojeiro¹¹, Gong-Bo Zhao^{13,11}

¹ Instituto de Física Teórica, (UAM/CSIC), Universidad Autónoma de Madrid, Cantoblanco, E-28049 Madrid, Spain

² Campus of International Excellence UAM+CSIC, Cantoblanco, E-28049 Madrid, Spain

³ Departamento de Física Teórica M8, Universidad Autónoma de Madrid (UAM), Cantoblanco, E-28049, Madrid, Spain

⁴ Instituto de Astrofísica de Andalucía (CSIC), Glorieta de la Astronomía, E-18080 Granada, Spain

⁵ CEA, Centre de Saclay, IRFU/SPP, F-91191 Gif-sur-Yvette, France

⁶ Center for Cosmology and Particle Physics, Department of Physics, New York University, NY 10003, New York, USA

⁷ Astronomy and Physics Departments and Theoretical Astrophysics Center, University of California, Berkeley, Berkeley CA 94720, USA

⁸ Astronomy Department, New Mexico State University, Las Cruces, NM, USA

⁹ Severo Ochoa Associate Researcher at the Instituto de Física Teórica (UAM/CSIC), Madrid, Spain

¹⁰ Center for Cosmology and AstroParticle Physics, The Ohio State University, Columbus, OH 43210, USA

¹¹ Institute of Cosmology & Gravitation, Dennis Sciama Building, University of Portsmouth, Portsmouth, PO1 3FX, UK

¹² School of Physics and Astronomy, University of St Andrews, North Haugh, St Andrews KY16 9SS, UK

¹³ National Astronomy Observatories, Chinese Academy of Science, Beijing, 100012, P.R.China

28 April 2022

ABSTRACT

In current and future surveys, quasars play a key role. The new data will extend our knowledge of the Universe as it will be used to better constrain the cosmological model at redshift $z > 1$ via baryon acoustic oscillation or modelling the redshift space distortion signal. Here, we present the first clustering study of the quasars observed by the extended Baryon Oscillation Spectroscopic Survey. We measure the clustering of $\sim 70,000$ quasars located in the redshift range $0.9 < z < 2.2$ that cover $1,168 \text{ deg}^2$. We model the clustering and produce high-fidelity quasar mock catalogues based on the BigMultiDark Planck simulation. In this aim, we use a modified (Sub)Halo Abundance Matching model to account for the specificities of the halo population hosting quasars. We find that quasars are hosted by halos with masses $\sim 10^{12.7} M_\odot$ and their bias evolves from 1.54 ($z = 1.06$) to 3.15 ($z = 1.98$). Using the current eBOSS data, we cannot distinguish between models with different fraction of satellites. The high-fidelity mock light-cones, including properties of halos hosting quasars, are made publicly available.

Key words: Cosmology: Large-scale structure of Universe – observations – quasars: general

1 INTRODUCTION

In modern cosmology, how quasars populate the large-scale structure is a puzzle. It is known that these objects trace the dark matter density field. Then, using measurements of the Baryon Acoustic Oscillations (BAO) or redshift space distortions (RSD) from quasars, one could infer information of the cosmological model. However, for these studies or for increasing the knowledge of the evolution of quasars, we require a good estimation of their distribution at all scales. In that way, spectroscopic surveys and high-

fidelity galaxy mocks from simulations are an important tool for solving many riddles concerning quasars.

Large galaxy spectroscopic surveys are an excellent tool to construct a precise 3D map of our Universe. These surveys allow studying the distribution of different populations in the Universe and constrain cosmological information via BAO scale or RSD. The Sloan Digital Sky Survey (SDSS; York et al. 2000) and the two degree field galaxy redshift survey (2dFGRS; Norberg et al. 2001) first measured the BAO scale in the local universe (Eisenstein et al. 2005; Cole et al. 2005). The Baryon Oscillation Spectroscopic Survey (Dawson et al. 2013, BOSS) included in the Sloan Digital Sky Survey III program (Eisenstein et al. 2011, SDSS-III) recently provided accurate redshifts for 1.5 million galaxies as faint as $i = 19.1$, that cover the redshift range $0.2 < z < 0.75$ on 10,000 square de-

* email: sergio.rodriguez@uam.es, Campus de Excelencia Internacional UAM/CSIC Scholar

† email: j.comparat@csic.es, Severo Ochoa Fellow

grees. Its combination with SDSS-I/II (York et al. 2000) provided a sub-percent level measurement of the BAO peak at redshift $z=0.57$ (Alam et al. 2016). SDSS has been an example of how spectroscopic surveys can provide strong constraints in our knowledge of the Universe.

Bright quasars constitute the best targets to sample the matter field at high redshift with a small exposure time. Indeed, quasars bear an Active Galactic Nucleus (AGN) that generates light which outshines the entire host galaxy. SDSS I/II published a sample of $\sim 100,000$ confirmed quasars (Schneider et al. 2010). SDSS-III observed $\sim 170,000$ quasars with redshift $2.1 < z < 3.5$ as faint as $g = 22$ (Pâris et al. 2014). Using both samples, the BAO feature was measured to a few per cents in the Lyman- α ($\text{Ly}\alpha$) forest (Font-Ribera et al. 2014; Delubac et al. 2015). Despite the large sample of quasars observed by the SDSS programs, there still is a large region in redshift ($1 < z < 2.1$) that ought to be studied by targeting quasars fainter than $i = 19.1$ in the SDSS imaging. Recent data from other experiments (Wright et al. 2010, e.g., WISE) provides additional information to best target quasars. A cutting-edge target selection algorithm was implemented in Myers et al. (2015) and is being observed by the extended Baryon Oscillation Spectroscopic Survey (eBOSS; Dawson et al. 2016), part of the SDSS-IV program. It will increase by a factor of five the number of quasars found by SDSS I/II in the redshift range $0.9 < z < 2.2$. This new sample will cover $\sim 7,500 \text{ deg}^2$, increasing both the volume and the low number density of the previous samples. It is designed to measure the BAO scale with quasars as tracers of the matter field. In this study, we consider the eBOSS First Year QSO data (hereafter Y1Q), for more details, see Section 2.1.

Different models have been used to analyse the clustering of quasars. In the literature, many studies focus on the linear regime (large scales). At these scales, correlation function can be described by a power-law (see e.g., Chehade et al. 2016, mostly due to the intrinsic low density of quasars). A more sophisticated method to model the galaxy clustering and generate mock catalogues is the Halo Occupation Distribution (HOD; Jing et al. 1998; Peacock & Smith 2000; Scoccimarro et al. 2001; Berlind & Weinberg 2002; Cooray & Sheth 2002; Zheng et al. 2005). The HOD model recovers the quasar clustering, but its parameters are largely degenerated, producing poor constraints on the host halo masses and satellite fraction (Richardson et al. 2012; Shen et al. 2013). Galaxy samples have also been studied with another method, namely halo abundance matching (HAM), which reproduces the clustering of complete galaxy samples with a reasonable agreement (e.g., Kravtsov et al. 2004; Conroy et al. 2006; Behroozi et al. 2010; Guo et al. 2010; Trujillo-Gomez et al. 2011; Nuza et al. 2013; Reddick et al. 2013). By including the stellar mass function (or luminosity function) the HAM accounts as well for incomplete samples (see e.g. Rodríguez-Torres et al. 2016). HAM requires knowledge on the stellar mass function, the scatter in the stellar mass to halo mass relation, and the incompleteness of the sample. In case of quasars, obtaining such information is not a easy task. However, modifications of the standard methods can be implemented to have a good description of the quasar distribution.

In the present study, we generate light-cones based on the BigMultiDark Planck simulation (BigMDPL; Klypin et al. 2014), using a modified HAM technique to reproduce the Y1Q clustering properties. The BigMDPL is an N -body simulation with box size $2.5 h^{-1} \text{ Gpc}$ and 3840^3 particles, which yields a volume large enough to encompass Y1Q. A variety of mocks, which model different populations of galaxies, have already been constructed using the BigMDPL simulation. They predict with a good agreement

the observed 2-point and 3-point statistics (Favole et al. 2015; Guo et al. 2015; Rodríguez-Torres et al. 2016).

This paper is structured as follows. In Section 2.3 we describe the data used in our analysis. Section 3 presents the different steps for constructing the BigMDPL eBOSS quasar mocks. Then, we populate dark-matter halos with a modified HAM algorithm that is described in Section 3.1. A set of predictions from our model is shown in Section 4. Subsequently, we discuss and summarise the most relevant results in Section 5 and Section 6. Throughout this work, we use the PLANCK-I cosmological parameters $\Omega_m = 0.307$, $\Omega_B = 0.048$, $\Omega_\Lambda = 0.693$ (Planck Collaboration et al. 2014).

2 DATA

2.1 eBOSS QSO survey and clustering

The eBOSS (Dawson et al. 2016) is part of the 6-years SDSS-IV program (fall 2014 to spring 2020), that combines the potential of SDSS-III/BOSS and new photometric information to optimise target selection and extend the BAO studies at higher redshift. eBOSS uses the 2.5-m Sloan Foundation Telescope at Apache Point Observatory (Gunn et al. 2006), and the same fibre-fed optical spectrograph used by BOSS, where each fibre subtends a $2''$ diameter on sky (Smee et al. 2013). This survey will provide redshifts for 300,000 Luminous Red Galaxies (LRG) in the redshift range $0.6 < z < 1.0$, a new sample of $\sim 200,000$ Emission Line Galaxies (ELG) at redshift $z > 0.6$, more than 500,000 spectroscopically-confirmed quasars at $0.9 < z < 2.2$ and $\sim 120,000$ new $\text{Ly}\alpha$ forest quasars at redshift $z > 2.1$.

The eBOSS dedicates 1,800 plates to cover an area of $9,000 \text{ deg}^2$: 1,500 plates to measure LRG and QSO redshifts on $7,500 \text{ deg}^2$ and 300 plates to measure ELG redshifts on $1,000 \text{ deg}^2$. The first two years, observations were dedicated to the QSO and LRG samples. In order to maximise the tiling completeness and fibre efficiency in the LRG/QSO sample, a tiered-priority is adopted (Dawson et al. 2016), where the QSO targets have maximal priority and are assigned to fibre first.

eBOSS has adopted two approaches to target quasars for redshift > 0.9 (Myers et al. 2015). “Clustering” quasar targets (qso_core) are used as a direct tracer of the large-scale structure in the redshift range $0.9 < z < 2.2$. The second approach is to detect quasars at $z > 2.1$ to map the large-scale structure via absorption of the $\text{Ly}\alpha$ forest (Palanque-Delabrouille et al. 2016).

(i) The CORE quasar sample is constructed combining optical selection in *ugriz* using a likelihood-based routine called XDQSOz (Bovy et al. 2011), with a midIR-optical colour-cut. eBOSS CORE selection (to $g < 22$ OR $r < 22$) should return ~ 70 quasars per sq. deg. at redshifts $0.9 < z < 2.2$ and about 7 quasars deg^{-2} at $z > 2.2$.

(ii) The $\text{Ly}\alpha$ quasar selection is based on variability in multi-epoch imaging from the Palomar Transient Factory (Palanque-Delabrouille et al. 2016). It should recover an additional 3 or 4 deg^{-2} $z > 2.2$ quasars to $g < 22.5$. A linear model of how imaging systematics affect target density recovers the angular distribution of eBOSS CORE quasars over 96.7% (76.7%) of the SDSS North (South) Galactic Cap area.

Busca et al. (2013) measure the BAO scale using $\text{Ly}\alpha$ quasars from the BOSS data. Font-Ribera et al. (2014) also give measurements of this scale using the cross correlation between visually confirmed quasars with the $\text{Ly}\alpha$ forest absorption. One of the goals of eBOSS is to provide a first detection of the BAO scale using

Table 1. Distribution of the Y1Q sample in four redshift bins. \bar{n} represents the comoving number density of QSO, N the number of QSO and V is the comoving volume of the redshift bin subtended by 1168 deg^2 . The last line shows values for the complete sample.

Redshift bin	\bar{n} [$10^{-5} \text{ Mpc}^{-3} h^3$]	N	V [$10^9 h^{-3} \text{ Mpc}^3$]
$0.9 < z < 1.2$	1.36	13,484	0.99
$1.2 < z < 1.5$	1.48	17,578	1.19
$1.5 < z < 1.8$	1.36	17,778	1.31
$1.8 < z < 2.2$	1.05	19,429	1.84
$0.9 < z < 2.2$	1.28	68,269	5.34

only the CORE quasar sample. In this context, we focus our study in the spectroscopically confirmed QSO using the Y1Q data which includes 68,269 objects that cover 1168 deg^2 . Table 1 shows the abundance of QSO for different redshift ranges.

2.2 Redshift error and statistical weights

The eBOSS project expects a redshift precision better than $300 \text{ s}^{-1} \text{ km}$ RMS for the QSO CORE at $z < 1.5$ and better than $[300+400(z-1.5)] \text{ km s}^{-1}$ at $z > 1.5$ (Myers et al. 2015). It corresponds to redshift errors of the order of 1×10^{-3} for $z < 1.5$ and $\sim 5 \times 10^{-3}$ for larger redshift. We add redshift errors in the mock catalogues using these upper limits. Indeed, it has an important impact on scales smaller than $10 h^{-1} \text{ Mpc}$ (see Appendix B). Finally, it is expected less than 1% of catastrophic error in the sample.

In order to include the observed redshift precision in the light-cones, we model redshift errors using a Gaussian distribution with mean value z_{true} and width Δz ,

$$z = z_{\text{true}} + \Delta z \mathcal{N}(0, 1), \quad (1)$$

where $\mathcal{N}(0, 1)$ is a random number coming from a Gaussian distribution with mean 0 and standard deviation 1, and

$$\Delta z = \begin{cases} 300 \text{ km s}^{-1} c^{-1} & \text{if } z < 1.5 \\ [300 + 400(z - 1.5)] \text{ km s}^{-1} c^{-1} & \text{if } z \geq 1.5, \end{cases} \quad (2)$$

here, c represents the speed of light. In addition, we include 1% of catastrophic redshifts, which introduces a boost in the correlation function of $\sim 1\%$ in all scales. (Appendix B).

A correct estimation of errors is important in order to understand the behaviour of the clustering at small scales. The monopole of the correlation function is affected over 50% for scales below $10 h^{-1} \text{ Mpc}$ because of redshift errors. The impact is larger in the quadrupole, where effects are detected at scales below $40 h^{-1} \text{ Mpc}$ (Reid & White 2011). In Appendix B we explore with more detail the impact of the errors in the clustering measurements. Even if we introduce a model for redshift errors, this is still an approximation which introduces unphysical effects in the estimation of the parameters of the model if small scales are included in the fitting. For this reason, we find the best parameters to reproduce the clustering between 10 and $40 h^{-1} \text{ Mpc}$, where the impact of redshift errors decreases and the effects of the cosmic variance and shot noise become smaller (Appendix B).

The $5\text{-}\sigma$ detection limit for point sources (also called depth) of the SDSS photometric survey varies across the footprint and differs for each band. The amplitude of the variations implies that faint targets end up very close to the detection limit. These targets are then more likely to be missed by the target selection algorithm.

eBOSS correct this effect by applying to the each quasar a depth-dependent weight, called ‘systematics weight’ w_{sys} (see Laurent et al. in prep for a detailed description).

In addition, the fiber collision effect and redshift failures are corrected by using close pair weights, w_{cp} and w_{zf} respectively. Those quantities are initialised to one for all objects, then, if a quasar has a nearest neighbour with a redshift failure or its redshift was not obtained because it was in a close pair, w_{zf} or w_{cp} are increased by one (Ross et al. 2012). The total weight for each quasar in the observed data is given by

$$w_{\text{Q}} = w_{\text{FKP}} w_{\text{sys}} (w_{\text{cp}} + w_{\text{zf}} - 1), \quad (3)$$

where w_{FKP} is the density weight applied for an optimal estimation of the 2-pt function and is defined by the expression (Feldman et al. 1994).

$$w_{\text{FKP}} = \frac{1}{1 + n(z) P_{\text{FKP}}}, \quad (4)$$

here $n(z)$ is the number density at redshift z and $P_{\text{FKP}} = 6000 h^{-3} \text{ Mpc}^3$.

Corrections of fiber collision by using close pair weights do not provide an accurate clustering signal at small scales (Guo et al. 2012; Hahn et al. 2016). However, in the quasar sample the distribution of objects is disperse and the number of collided pairs is very small. Additionally, our analysis does not use scales below $10 h^{-1} \text{ Mpc}$, hence, the close pair correction is good enough for our purpose. In case of simulated quasars, we only include FKP weights to compute the 2-point statistics, $w_{\text{sim}} = w_{\text{FKP}}$.

2.3 The eBOSS BigMultiDark light-cone

The suite of MultiDark¹ Planck simulations adopts a flat Λ CDM model with PLANCK-I (Planck Collaboration et al. 2014) cosmological parameters: $\Omega_m = 0.307$, $\Omega_B = 0.048$, $\Omega_\Lambda = 0.693$, $\sigma_8 = 0.829$, $n_s = 0.96$ and a dimensionless Hubble parameter $h = 0.678$. We use two of the N -body simulations described in Klypin et al. (2014). The BigMultiDark (BigMDPL) has a box length of $2.5 h^{-1} \text{ Gpc}$, and 3840^3 particles of mass $2.4 \times 10^{10} h^{-1} M_\odot$. The MultiDark Planck (MDPL) has a box length of $1.0 h^{-1} \text{ Gpc}$ and 3840^3 particles with a mass of $1.5 \times 10^9 h^{-1} M_\odot$. Both were built with GADGET-2 (Springel 2005) using initial Gaussian fluctuations generated with the Zel’dovich approximation at redshift 100.

From the dark matter catalogues of the simulation, halos are defined with the ROCKSTAR (Robust Overdensity Calculation using K-Space Topologically Adaptive Refinement) halo finder (Behroozi et al. 2013). Spherical dark matter halos and sub-halos are identified using an approach based on adaptive hierarchical refinement of friends-of-friends groups in six phase-space dimensions and one time dimension. ROCKSTAR computes halo mass using spherical overdensities of a virial structure (Bryan & Norman 1998). Before calculating halo masses and circular velocities, the halo finder performs a procedure which removes unbound particles from the final mass of the halo². We include observational effects and construct a catalogue with similar volume to the eBOSS sample, by making light-cones based on different snapshots of the BigMDPL simulation.

We perform the abundance matching using the maximum circular velocity of the halo (V_{max}) to link dark matter halos and

¹ <http://www.multidark.org/>

² <http://www.cosmosim.org/>

quasars. The maximum circular velocity is one of the best candidates for matching dark matter halos and galaxies (Reddick et al. 2013). V_{max} relates with the virial mass of the halo through a power-law given by

$$V_{max} = \beta(z)[M_{vir}E(z)/(10^{12}h^{-1}\text{Mpc})]^{\alpha(z)}, \quad (5)$$

where, $E(z) = \sqrt{\Omega_{\Lambda,0} + \Omega_{m,0}(1+z)^3}$, $\log_{10}\beta(z) = 2.209 + 0.060a - 0.021a^2$ and $\alpha(z) = 0.346 - 0.059a + 0.025a^2$, with $a = 1/(1+z)$ the scale factor (see Rodríguez-Puebla et al. 2016). Although there are better candidates to perform the matching between dark matter halos and galaxies, such as the maximum circular velocity along the whole history of the halo (V_{peak}), the BigMDPL simulation has a small number of snapshots in the quasar redshift range (4). This relatively small number of time-steps prevents to have a good estimation of quantities that are computed by tracing halos between snapshots. For this reason, we use V_{max} to implement our model. Differences between V_{peak} and V_{max} become important in case of substructures, while the selection of host halos is similar with both quantities. Reddick et al. (2013) show a significantly larger amount of subhalos when V_{peak} is used rather than other quantities. However, in our model the impact of choosing V_{max} can be compensated by using the fraction of satellites as a free parameter. Furthermore, the poor information of the one halo term in the quasar sample and the large errors in observations will not allow distinguishing which quantity performs better the matching.

Table 2 presents the deviation of each simulation from a model of the complete mass function, which is obtained by fitting a data set that contains the complete part of each of the MultiDark Planck simulation (SMDPL, MDPL, BigMDPL, HMDPL). Masses in Table 2 fulfil the condition given by

$$N_{sim}(M_{200} > M_i)/N_{mod}(M_{200} > M_i) < \text{percentage}, \quad (6)$$

where N_{sim} is the number of objects in the simulation with M_{200} smaller than the threshold mass M_i and N_{mod} is the corresponding number of halos in the model. Previous works showed that quasars live in halos with masses of the order of $\log(M/M_{\odot}) \sim 12.5$ (Shen et al. 2013; Chehade et al. 2016). Both simulations mentioned above are complete for this mass as is shown in Table 2. But depending on the dispersion of the distribution of halos hosting QSO, a small fraction of halos coming from the incomplete part of the simulation enter in the final mock. We quantify the effect of the resolution on our catalogues with the MDPL, where this effect is negligible thanks to its higher resolution. MDPL has enough resolution to cover the halo mass range for the QSO population; however, its volume is smaller than the one covered by eBOSS, so one cannot construct a complete light-cone without box replications. In addition, the shot noise from a mock using this volume is very large, due to the low number density of the observed sample. In Appendix A, we show this effect by comparing the mocks generated from both simulations.

We include the evolution with redshift of the number density and of the clustering. The light-cone constructed with BigMDPL in the range $0.9 < z < 2.2$ covers $1,481.75 \text{ deg}^2$, which is comparable with Y1Q. The mocks are constructed with the SURvey GenerAtor code (SUGAR; Rodríguez-Torres et al. 2016). In this procedure, we use all available snapshots from the BigMDPL simulation ($z = 2.145, 1.445, 1, 0.8868$) and from the MultiDark simulation we select only the closest snapshots to study the effects of the incompleteness ($z = 1.425, 0.987$, see Appendix A). We present results from three different light-cones, the first one uses a single set of parameters to describe the Y1Q (BigMDPL-QSO light-cone). The second one is obtained by fitting the clustering in four redshift bins

with different set of parameters (BigMDPL-QSOZ light-cone). The last light-cone uses a single set of parameters, but only host halos are included (fraction of substructures equal to zero, BigMDPL-QSO-NSAT).

2.4 Galaxy Mocks for QSO (GLAM)

In order to estimate the uncertainties in the clustering measurements, we use the GaLAXy Mocks (GLAM) scheme for the eBOSS quasar sample, which, for this application, implements a new parallel particle mesh method (PPM-GLAM; Klypin & Prada, in prep.) to construct the dark matter density field, and an optimisation to populate the simulation with quasars (Comparat et al., in prep.). We run the SUGAR-code to construct light-cones (Rodríguez-Torres et al. 2016). Errors are extracted from the diagonal terms of the covariance matrix from 1000 GLAM-QSO mocks which cover the same area as the data. We use the covariance matrix estimator given by

$$C_{ij} = \frac{1}{n_s - 1} \sum_{k=1}^{n_s} (x_i^k - \mu_i)(x_j^k - \mu_j), \quad (7)$$

where n_s is the total number of mocks and the mean of each measurement is

$$\mu_i = \frac{1}{n_s} \sum_{k=0}^{n_s} x_i^k. \quad (8)$$

Using the covariance matrix from these mocks we perform the fitting with the χ^2 statistics,

$$\chi^2 = \sum_{ij} [x_i^d - x_i^m] C_{ij}^{-1} [x_j^d - x_j^m], \quad (9)$$

where x_i^m and x_i^d are the measurements (ξ_0, ξ_2, w_p, P_k) from the model and the data in the bin i respectively. χ^2 values presented in this work are computed from the monopole of the correlation function.

3 CLUSTERING MODEL

The best way to study the observed clustering of a survey would be to simulate not only the effect of the gravity on the dark matter but also on the baryonic matter, and that would include stellar physics to provide a direct prediction of the relation between dark matter halos and the galaxies and their evolution with time. This approach is undertaken by hydrodynamical simulations, that include galaxy formation processes, stellar physics and AGN feedback. EAGLE (Rahmati et al. 2015) and ILLUSTRIS (Sijacki et al. 2015) are two of the most recent realisations which predict a realistic distribution of galaxies and quasar populations. However, those simulations are constructed in rather small boxes of $\sim 75h^{-1} \text{ Mpc}$, which impedes studies of the large scale structure. The large amount of computational resources in hydrodynamic simulation is prohibitive and the computation of volumes comparable to observations nearly infeasible.

An alternative approach, cheaper in computational time, is to use the dark matter only simulations and add the galaxies in a statistical way. There are two widely used models based on these statistical relations. The first one is the Halo Occupation Distribution (HOD; e.g., Guo et al. 2014), which gives the probability, $P(N|M_h)$, that a halo of mass M_h hosts N galaxies. This probability is described by a fitting formula, which is fixed using the clustering

Table 2. Deviation from the mass function at redshift 0 for the MDPL and the BigMDPL simulations. The masses and the maximum circular velocities are the threshold above which the completeness in this box relative to the mass function is higher than the percentage given in the header. In parenthesis is given the corresponding number of particles.

fraction	$\log(M_{200c}(z)/M_\odot)$				V_{max}			
	80%	90%	95%	97%	80%	90%	95%	97%
central halos								
MDPL	11.035 (71)	11.095 (82)	11.255 (119)	11.605 (266)	57.34	68.62	98.28	121.92
BigMD	12.215 (69)	12.275 (79)	12.315 (87)	12.365 (98)	131.00	145.91	201.60	299.28

measurements from the observational data. The second method to populate the dark matter halos is the Halo Abundance Matching (HAM; e.g., Reddick et al. 2013). This model assumes that most massive galaxies populate the most massive halos.

3.1 The modified SHAM model

Favole et al. (2015) introduced a modified (Sub) Halo Abundance Matching (SHAM), designed to reproduce the clustering of the ELG sample from BOSS. They select halos from the simulation using a probability function, which is the sum of one term corresponding to host halos and the other one to satellites halos. This probability is a Gaussian function that has three parameters: the mean mass, the width of the distribution and the satellite fraction. To model the observed Y1Q clustering, we use a similar model. Indeed, the QSO sample is not complete in halo mass or stellar mass whatsoever. Instead of using the virial mass of halos, we use V_{max} and assume that the distribution of halos hosting quasars has a Gaussian shape. The most general model is split in central and satellites as done in Favole et al. (2015). When a QSO is located in the centre of a host halos, it is denoted as a central QSO. The satellite fraction refers to the fraction of QSO living in a sub-halo. This fraction does not represent systems of binary quasars. The central halo that is the counterpart of a satellite QSO can host another kind of galaxy.

In case of quasars, we do not use the luminosity of the observed sample. Our model only uses the V_{max} distribution of halos, as done by Nuza et al. (2013). Rodríguez-Torres et al. (2016) extend the HAM procedure implemented by Nuza et al. (2013) using the stellar mass function and modelling the incompleteness of the sample. In that study, galaxies are assigned to halos via a standard HAM and then they are downsampled to obtain the observed stellar mass distribution. Here, we assume that the intrinsic scatter between quasars and dark matter halos, plus the incompleteness of the sample will produce a V_{max} distribution with a Gaussian shape. Then the model orders halos by V_{max} and downsamples objects as done by Rodríguez-Torres et al. (2016).

3.2 Implementation

Assuming that the final V_{max} distribution of the simulated quasar catalogue is Gaussian, we need to construct a probability distribution function, which selects halos from the complete simulation based on this condition. In a general case the V_{max} distribution of the final catalogue will be

$$\begin{aligned}
 \phi_{QSO}(V_{max}) &= \phi_{QSO}^s + \phi_{QSO}^c \\
 &= P_s(V_{max})\phi_{sim}^s(V_{max}) + P_c(V_{max})\phi_{sim}^c(V_{max}) \\
 &= \mathcal{G}_s(V_{max}) + \mathcal{G}_c(V_{max}),
 \end{aligned}$$

where ϕ_{sim}^c and ϕ_{sim}^s represent the V_{max} distribution of host halos and subhalos respectively and \mathcal{G}_s and \mathcal{G}_c are Gaussian functions with mean V_{mean} , standard deviation $\sigma_{V_{max}}$, and each one is normalised using

$$\int \mathcal{G}_s(V_{max}, z) dV_{max} = N_{tot}(z) f_{sat}$$

$$\int \mathcal{G}_c(V_{max}, z) dV_{max} = N_{tot}(z) (1 - f_{sat})$$

here $N_{tot}(z)$ is the total number of quasars per redshift bin given by the observed number density.

In order to construct the probability distribution, we sort all halos in the simulation and compute (separately) the maximum circular velocity function (V_{max}) for sub-halos and halos. Using the fraction of satellites as a free parameter and the number density observed in the data, we normalise the sum of the Gaussian of the central and the satellites. We divide the halos in bins of V_{max} and compute the probability of assigning a quasar to a dark matter halo (central or satellite) per bin as

$$P_{s/c}(V_{max}) = \frac{N_{s/c}^{gaus}}{N_{sub/host}^{tot}}, \quad (10)$$

where $N_{sub/host}^{tot}$ is the total number of sub/host halos in the range $[V_{max} - \Delta V_{max}/2, V_{max} + \Delta V_{max}/2]$ and $N_{s/c}^{gaus}$ is the number of satellite/central quasars necessary to produce the final Gaussian shape. Using equation (10) we downsample all halos in the simulation to obtain a QSO catalogue.

Our model consists of 5 different parameters, the mean and standard deviation values for satellite and central distributions and the fraction of satellites. However, we assume the same mean and standard deviation for central and satellites. In addition, due to the current data, we do not have enough information at small scales ($< 1.0 h^{-1} \text{Mpc}$) to extract precise information about the standard deviation of the distribution and the satellite fraction of the eBOSS QSO sample. For these reasons, our unique parameter to fit the clustering is the mean value of the distribution (V_{mean}).

3.3 Parameters

The three parameters of the model are V_{mean} , σ_{max} and f_{sat} . Juast as Favole et al. (2015), we do not find a dependency of the clustering with the width of the Gaussian distribution. Figure 2 shows the χ^2 maps obtained when varying V_{mean} , σ_{max} and f_{sat} , neither σ_{max} nor f_{sat} are constrained with current data. In the mass regime where QSO live, σ_{max} impacts the clustering at small scales ($< 0.5 h^{-1} \text{Mpc}$), for this reason we cannot constrain this parameter. At scales larger than $1.0 h^{-1} \text{Mpc}$ the clustering amplitude only depends on V_{mean} . The model shown in Chehade et al. (2016) is consistent with a width in halo mass of $\sigma_{max} = 45 \text{ km s}^{-1}$. Due to the resolution

Table 3. Results of the fit per redshift bin. A gives the area in deg^2 subtended by the mock light-cone. z bin gives the lower and upper boundary of the redshift bin. V_{mean} is the best fit parameter found. $\log_{10}(M_{200}/M_{\odot})$ is the corresponding mean \pm standard deviation of the halo mass of the population selected. χ_r^2 is the reduced χ^2 per 9 degrees of freedom. We fixed $\sigma_{\text{max}} = 30 \text{ km s}^{-1}$ and f_{sat} is fixed to the natural value found in the simulation.

A (deg^2)	z bin	V_{mean} (s^{-1}km)	$\log_{10}(M_{200}/M_{\odot})$	χ_r^2
BigMDPL-QSO				
1,481.75	0.9 – 2.2	341.18 \pm 30.01	12.66 \pm 0.16	1.78
BigMDPL-QSOZ				
3,275.06	0.9 – 1.2	282.83 \pm 30.16	12.53 \pm 0.17	1.47
2,371.81	1.2 – 1.5	324.13 \pm 30.11	12.63 \pm 0.14	1.85
1,879.13	1.5 – 1.8	339.53 \pm 29.87	12.69 \pm 0.14	1.70
1,481.75	1.8 – 2.2	353.51 \pm 29.72	12.60 \pm 0.13	2.24
BigMDPL-QSO-NSAT				
1,481.75	0.9 – 2.2	349.48 \pm 30.26	12.70 \pm 0.16	1.52

of BigMultiDark, we decrease this value to $\sigma_{\text{max}} = 30 \text{ km s}^{-1}$. This ensures the BigMDPL-QSO and the BigMDPL-QSOZ light-cones have $\sim 2\%$ halos in the region where the incompleteness is larger than 10%. Since we cannot fit the satellite fraction, we do not distinguish between central and satellite when randomly sampling for halos.

4 RESULTS

We compare the Y1Q 2-point correlation function (2PCF) with that of the mocks for a grid parameters using the χ^2 statistics with 9 degrees of freedom. In order to compute the 2PCF we use a modified version of the Correlation Utilities and Two-point Estimation code (CUTE; Alonso 2012). We first analyse the complete sample ($0.9 < z < 2.2$). We find the best value for the parameter $V_{\text{mean}} = 341.18 \text{ km s}^{-1}$, which corresponds to a sample of mock QSO with mean mass $\log[M_{200}/M_{\odot}] = 12.66 \pm 0.16$. Fig. 1 presents the clustering measurements (2PCF and power spectrum) along with the prediction of the best-fit mock light-cone. The agreement between data and model is excellent.

When fitting the parameters using the clustering of the complete redshift range, the evolution of the mass distribution is not taken into account. We investigate this effect and divide the sample in four redshift bins and fit parameters to match the clustering in individual redshift bin. It improves slightly the quality of the fits, see Table 3. This Table gives the best fit values of the V_{mean} parameters and the corresponding reduced χ^2 .

Comparing the values of M_{200} presented in the Table 3 with that of Table 2, we infer that the best fit mocks have less than 1% of objects taken from a bin where the completeness is lower than 90%. The effect of the resolution on the clustering is discussed in more detail in Appendix A.

We find the satellite fraction, f_{sat} , to be degenerated with V_{mean} , and this degeneracy is broken only with information from the one halo term. However, the current Y1Q data does not allow going to those scales. In Fig. 2, we present the χ^2 maps we obtain for different combinations of the three parameters V_{mean} , σ_{max} and f_{sat} . The left hand panel shows that the satellite fraction is not constrained. For this reason, we do not fix the number of satellite in two of the three mocks presented, which means that host halos and

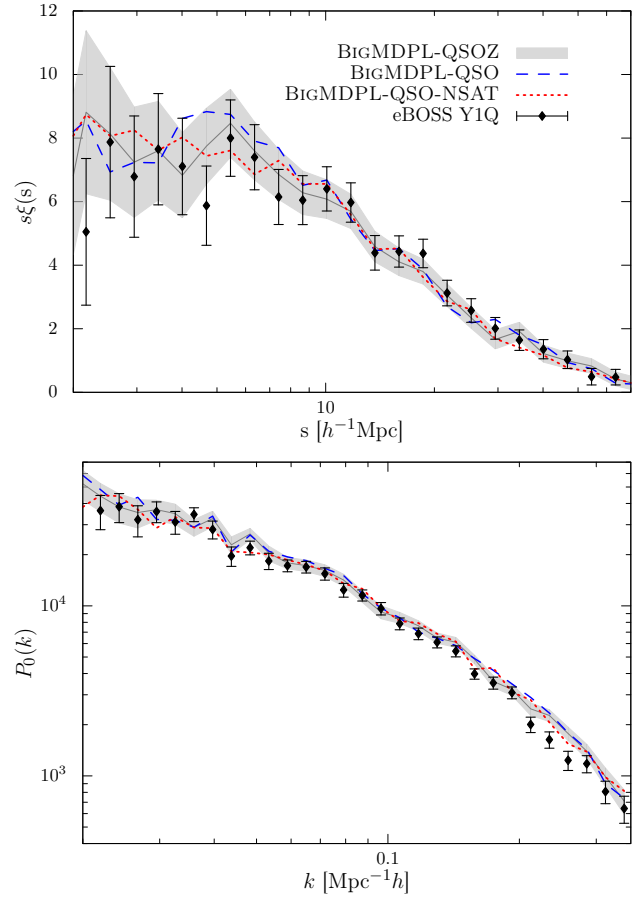


Figure 1. Top panel: Monopole of the correlation function in configuration space of Y1Q (points with errors-bars). The shaded area represents the BigMDPL-QSOZ light-cone fitted in four different redshift bins. Dashed line represents the BigMDPL-QSO light-cone fitted on a single redshift bin and dotted line is the BigMDPL-QSO-NSAT. Bottom panel: Monopole of power spectrum of the Y1Q (points with errors-bars) and the three BigMDPL light-cone. The agreement between the best model and the data is remarkable. Errors-bars and dash areas are computed using 1000 GLAM catalogues. Differences at high k are due to redshift errors.

satellite halos are not distinguished when selection is implemented. Then, the fraction of satellites in the mock has the same dependency with V_{max} as the complete simulation. The third light-cone with $f_{\text{sat}} = 0$ is included to show the impact of removing all substructures from the analysis. The second parameter of the model, σ_{max} is also not constrained (see Figure 2). A similar problem was found by Shen et al. (2013), their HOD parameters are largely degenerated, and the fraction of satellites is not well constrained. For these reasons, we only vary the mean value of the Gaussian distribution (V_{mean}) to fix the clustering of the model.

4.1 Trends of the QSO clustering with redshift

The signal of the clustering of the QSO sample does not have an important evolution, as shown in Figure 3, the monopole varies mildly in the linear regime in all four redshift bins. If we assume a constant distribution of V_{max} for the whole redshift range, the evolution of the dark matter field will produce a non-constant signal of clustering in the different redshifts. In order to reproduce the observed

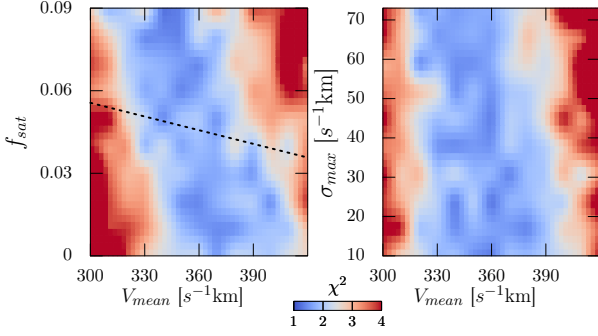


Figure 2. χ^2 maps for the three parameters of the model implemented on the BigMDPL-QSO. The left-hand panel shows the satellite fraction vs. V_{mean} , it is possible to note a degeneracy between both parameters. For that reason, we use the f_{sat} given by the simulation (dotted line). The right-hand panel presents σ_{max} vs. V_{mean} , σ_{max} cannot be constrained using the current data.

evolution and predict a most realistic linear bias we divide the complete redshift range in four regions fitting the clustering of the light-cone to the one observed in each bin. Table 3 presents the redshift range and the best-fit parameter found to match the observed data. We use different areas for each redshift bin to maximise the volume used from the simulation. These larger areas increase the statistics and reduce the shot-noise in the 2PCF of the mocks; see Table 3.

Figure 1 shows the monopole of the correlation function and the power spectrum of the three different mocks (BigMDPL-QSO/QSOZ/QSO-NSAT) compared to the observed data for the whole redshift range. All light-cones can reproduce with a good agreement the eBOSS data. The BigMDPL light-cones have shot-noise and cosmic variance similar to the data. Due to those large errors in the model and the data, it is difficult to distinguish which light-cone reproduces better the data in the complete redshift range. However, if the model reproduces the clustering at different redshifts, we can estimate with better accuracy the evolution of the bias.

In order to quantify the difference between both models (BigMDPL-QSO and BigMDPL-QSOZ), we compare both methods using the Bayes factor. We can compute it through the maximum-likelihood

$$P(\mathbf{x}|\mathbf{p}) = \frac{|\tilde{\mathbf{C}}^{-1}|}{(2\pi)^p} \exp \left[-\frac{1}{2} \sum_{ij} (x_i^d - x_i(\mathbf{p})) \tilde{C}_{ij}^{-1} (x_j^d - x_j(\mathbf{p})) \right] \quad (11)$$

where x^d represents the data and $x(\mathbf{p})$ the model. We estimate the inverse covariance matrix using equation (7) and correcting for bias using Hartlap factor (Hartlap et al. 2007)

$$\tilde{C}_{ij}^{-1} = \frac{N_{\text{mock}} - N_p - 2}{N_{\text{mock}} - 1} C_{ij}^{-1} \quad (12)$$

here, N_p represent the number of data points used. The Bayes factor between the BigMDPL-QSO and the BigMDPL-QSOZ model is

$$K = \frac{P(\xi_{\text{data}}|\xi_{\text{qsoz}})}{P(\xi_{\text{data}}|\xi_{\text{qso}})} = 5.45. \quad (13)$$

This result suggests that BigMDPL-QSOZ model is more substantial supported by the data than BigMDPL-QSO. The Bayes factor between the BigMDPL-QSOZ and the BigMDPL-QSO-NSAT is $K=1.67$. In this case we cannot conclude which model reproduce better the data. However, the BigMDPL light-cones have an

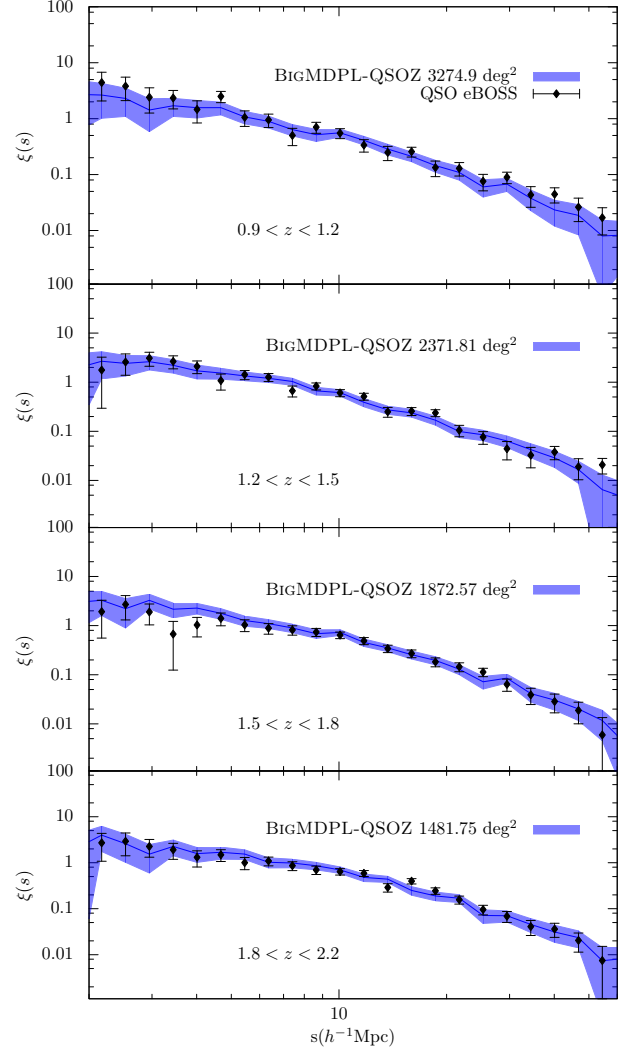


Figure 3. Monopole 2PCF vs. redshift. We show the Y1Q (points) and the best-fit mock (shaded area) of the BigMDPL-QSOZ light-cone (see Table 3). Each panel corresponds to a different redshift bin. Errors-bars and dash areas are computed using 1000 GLAM catalogues.

important variability between realisations when the random seed is changed and it is not possible to construct a sufficient number of independent light-cones to make a definitive statement about both models. In terms of χ^2 both models are in agreement with the current data, though including a model with more parameters will improve the fitting of the data.

4.2 Checking $\xi_2(s)$ and $w_p(r_p)$

The quadrupole is very sensitive to processes affecting the small scales. Effects due to fibre collision have an important impact at scales beyond the fibre size; however, the effect of fibre collision is very small in the QSO sample. The most important observational effect is due to redshift errors, as is seen in Appendix A. Figure 4 shows the quadrupole of the BigMDPL-QSO, BigMDPL-QSOZ and BigMDPL-QSO-NSAT light-cones compared to the observations. All light-cones reproduce the data within $1-\sigma$ error. This agreement suggests that the model used to account for redshift er-

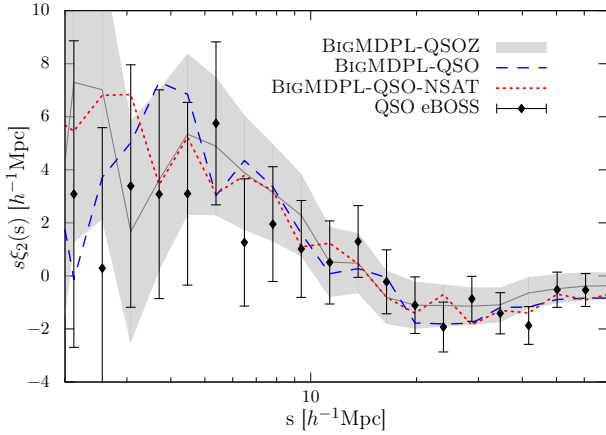


Figure 4. Quadrupole vs. comoving scale in redshift-space predicted by the BigMDPL-QSOZ (shaded region), BigMDPL-QSO (dashed line) and BigMDPL-QSO-NSAT (dotted lines) compared to the Y1Q (black points). All mocks are in agreement with observations. Errors-bars and shaded areas are computed using 1000 GLAM catalogues.

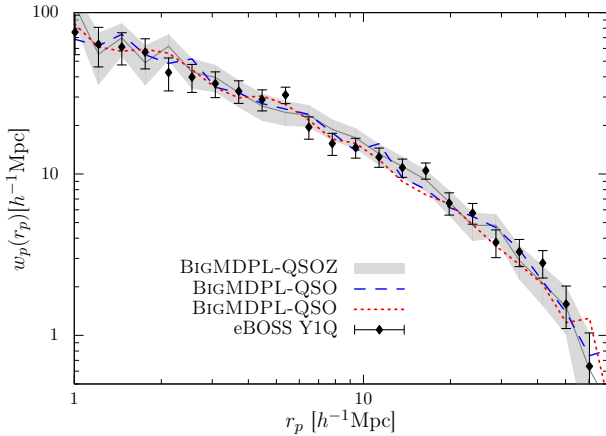


Figure 5. Projected correlation function predicted by the BigMDPL-QSOZ (shaded region), BigMDPL-QSO (dashed line) and BigMDPL-QSO-NSAT (dotted lines) compared to the Y1Q (black points). The width of the shaded area represents 1- σ errors, computed with 1000 GLAM catalogues. Our model reproduces the clustering for all relevant scales.

ror is reasonable. Note that the light-cone including the redshift evolution of the clustering reproduces best the quadrupole.

We compared the projected correlation function for the three light-cones and the observed data, finding a good agreement, see Fig. 5.

The clustering predicted by best model, which is mainly determined by the V_{mean} , reproduces with good agreement the 2-point statistics of the observed data. We do not find significant differences between the three light-cones presented, all of them can reproduce the 2-point statistics of the complete Y1Q sample with a good agreement.

4.3 Bias

Y1Q data allows for accurate measurements of the correlation function $\xi(r)$ and of the quasar bias b_Q , within the redshift range $0.9 <$

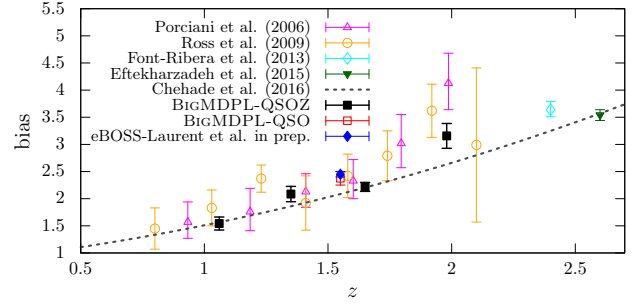


Figure 6. QSO bias as a function of redshift. The bias is computed using BigMDPL-QSOZ and BigMDPL-QSO light-cones. We include results from Chehade et al. (2016), Eftekharzadeh et al. (2015), Font-Ribera et al. (2014), Ross et al. (2009) and Porciani & Norberg (2006). eBOSS bias measurements are in agreement with previous results and about ten times more precise. Results of eBOSS from Laurent et al. in prep. are also included.

$z < 2.2$. Laurent et al. (in preparation) obtains $b_Q = 2.45 \pm 0.05$, when averaged over separations between 10 and $90 h^{-1}$ Mpc. This value is compatible with the previous SDSS measurements, $b_Q(z = 1.58) = 2.42 \pm 0.40$, by Ross et al. (2009).

We estimate the bias using the dark matter counter-part of the QSO mock light-cone. Using the autocorrelation of the dark matter sample, and the correlation function of the QSO mock in real space, we estimate the bias using

$$b(r)^2 = \frac{\xi(r)}{\xi_{DM}(r)}. \quad (14)$$

Figure 6 presents the bias of the BigMDPL-QSOZ and the BigMDPL-QSO compared to previous studies.

Figure 6 presents previous bias measurements from spectroscopically confirmed quasars in the two degree field (2dF; Porciani & Norberg 2006) at $0.8 < z < 2.1$, SDSS-I/II (Ross et al. 2009) at $z < 2.2$, the Quasar Dark Energy Survey pilot (2QDES; Chehade et al. 2016) for redshift between 0.8 and 2.5 and the BOSS sample (Eftekharzadeh et al. 2015) at $2.2 < z < 2.8$. All these studies parametrise the real space correlation function by a power-law, $\xi(r) = (r/r_0)^\gamma$, which can be related with the observed correlation function (redshift space) by

$$\xi(s) = \left(b_Q^2 + \frac{2}{3} b_Q f + \frac{f^2}{5} \right) \xi(r), \quad (15)$$

where $f = [\Omega_m(z)]^{0.56}$ is the gravitational growth factor. In addition, we include measurements of quasars via Lyman- α absorption at redshift 2.4 from the BOSS sample (Font-Ribera et al. 2014). Eftekharzadeh et al. (2015) also show a comparison between different estimations of the bias. At the redshifts studied, the bias measurements obtained in our study are in good agreement (see Figure 6) and they are a factor 5 to 10 times more precise than previous studies.

4.4 Cross-correlation coefficients

The linear bias provides a good description of the relationship between dark matter and QSO mock in the linear regime. However, a single parameter b_Q is not enough to understand the link between galaxies and dark matter at all scales. To parametrise this relationship, we use the second order bias, which is related to scales smaller than $10 h^{-1}$ Mpc. The second order bias is inferred from the cross

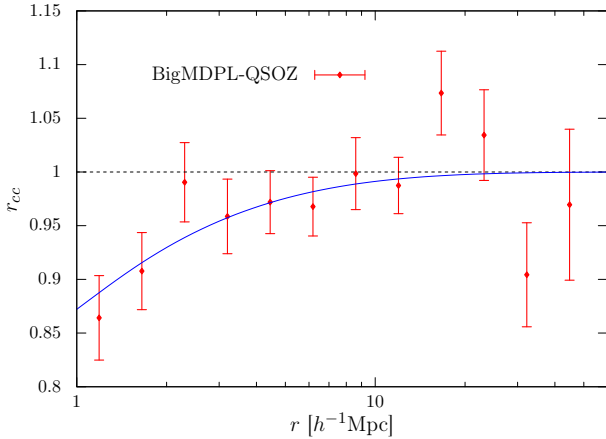


Figure 7. Cross-correlation coefficient between the dark matter field and the BigMDPL-QSOZ light-cone. The best model from (17) is shown with a solid line.

Table 4. Mean halo mass and satellite fraction prediction from the BigMDPL light-cones.

Light-cone	V_{mean} [$s^{-1} \text{Kpc}$]	$\log_{10}[M_{200}/M_{\odot}]$	f_{sat}
BigMDPL-QSOZ	326.94	12.61	0.048
BigMDPL-QSO	341.18	12.66	0.053
BigMDPL-QSO-NSAT	349.48	12.70	0.0

correlation coefficient. It gives an estimation of the correlation between the positions of quasars and the dark matter field (Dekel & Lahav 1999). The cross-correlation, denoted r_{cc} , between quasars and the dark matter field is defined as

$$r_{cc}(r) = \frac{\xi_{qm}(r)}{\sqrt{\xi_{qq}(r)\xi_{mm}(r)}}, \quad (16)$$

where q denotes the quasar sample and m the dark matter. r_{cc} is sensitive to the non-linear stochastic bias of the sample. Figure 7 shows the cross-correlation coefficient between BigMDPL-QSOZ and the dark matter field. For scales larger than $10 h^{-1} \text{Mpc}$, the cross-correlation function is consistent with 1. As expected, in this regime, we have $\xi_{gm} = b_Q \xi_{mm}$ and $\xi_{gg} = b_Q^2 \xi_{mm}$. At smaller separations, r_{cc} becomes smaller than unity. This tendency is described in perturbation theory Baldauf et al. (2010), where r_{cc} is described with the second order bias by

$$r_{cc}(r) \approx 1 - b_2^2 \frac{\xi_{lin}(r)}{4}, \quad (17)$$

where b_2 is the second order bias and ξ_{lin} is the linear correlation function. The cross-correlation coefficient is best fit by $b_2 = 0.314 \pm 0.030$. This relation is sufficient for the scales studied ($1 < rh^{-1} \text{Mpc} < 10$), see the solid line in Fig. 7.

4.5 Halo Occupation Distribution

The mean halo mass of halos hosting Y1Q QSOs and the satellite fraction characterise how QSO populate the dark matter halos. Table 5 shows the mean value of V_{max} , mean halo mass and satellite fraction for all light-cones built in this study.

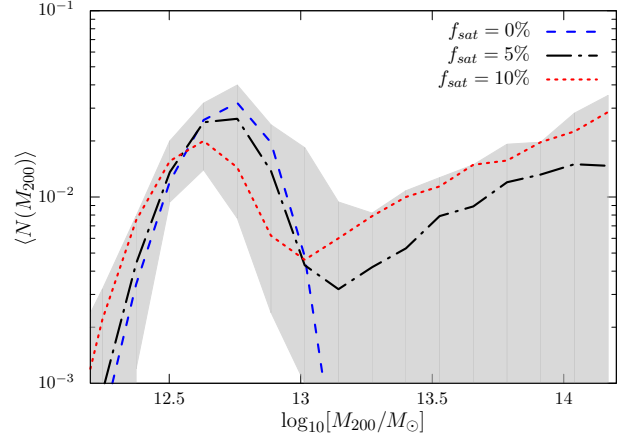


Figure 8. Halo Occupation distribution for central plus satellites predicted from the BigMDPL-QSO light-cone. We present three light-cones using different fraction of satellites. The shaded area is computed adding $1-\sigma$ error in the V_{mean} parameter for each light-cone. In addition, we vary the width of the distribution from 10 to $60 s^{-1} \text{km}$ to see the impact of this parameter in the HOD. f_{sat} is also changed from 0 to 0.12

If the satellite fraction is not fixed (no distinction between halos and sub halos), we obtain a non-negligible fraction of satellites, $\sim 5\%$, which is consistent with Shen et al. (2013) which find a satellite fraction of 6.8% . However, due to the degeneracy between V_{mean} and f_{sat} , our model could also match the clustering with a negligible fraction (Figure 2), as presented in Richardson et al. (2012).

Another way to formulate how QSO populate the density field is the probability of finding N quasars in a halo of mass M ($\langle N(M) \rangle$), namely the HOD model. This method describes with a set of parameters fit directly on the clustering how quasars would statistically populate halos. In SHAM models, $\langle N(M) \rangle$ is given by the halo catalogue by counting the total number of host halos and the number of QSO per bin of mass. Figure 8 shows the halo occupation distribution predicted by the BigMDPL-QSO light-cone. We use this light-cone rather than the other as it has a negligible fraction of objects from the incomplete part of the BigMDPL simulation. It also allows σ_{max} and f_{sat} to vary in a wide range, letting us show the dependency of $\langle N(M) \rangle$ on these parameters, see the different lines in Fig. 8.

We additionally construct light-cones with different V_{mean} including variation of $1-\sigma$ from the best-fit. In these, we also vary the width of the distribution between 10 and $60 s^{-1} \text{km}$. We do not use a larger σ_{peak} , because we do not want to include a large fraction of objects coming from the incomplete part of the simulation. f_{sat} is also varied between 0 and 10%. The shaded area in Figure 8 represents the all HODs encompasses by these parameter variations.

Compared to previous results using HOD (Shen et al. 2013), our model puts new constraints for masses below $10^{13} M_{\odot}$. We find a distribution dominated by the mean halo mass of the sample. However, $\langle N(M) \rangle$ has a strong dependency with the other two parameters of the model, which we cannot constrain with the current data. An improvement on small scales of the QSO clustering or the cross correlation between ELG and QSO in future surveys would constrain σ_{peak} and f_{sat} and therefore provide better HOD predictions.

5 DISCUSSION

Previous HOD analysis of the SDSS QSO sample combined different data sets to get more information about the distribution of QSOs inside halos. However, due to the large uncertainties in the data, the parameters of the HOD remain degenerated.

Richardson et al. (2012) studied the clustering of the 48,000 QSO from the SDSS sample in the redshift range $0.4 < z < 2.5$ and interprets the measurements of the projected correlation function at redshift 1.4. In addition, they use a sample of 4,426 spectroscopically identified quasars in the redshift interval $2.9 < z < 5.4$ from Shen et al. (2007) in order to have the small scales clustering, that cannot be measured directly from the SDSS QSO. However, they use a regular HOD without include duty cycle, which make that their parameters reproduce the clustering, but most of them are unphysical. Shen et al. (2013) studied the two-point cross-correlation function of 8,198 SDSS QSO and 349,608 BOSS CMASS galaxies in the redshift range $0.3 < z < 0.9$. The BOSS sample provides a set of CORE QSO, which were studied by (Eftekharzadeh et al. 2015). They extend the analysis of the projected correlation function of the BOSS sample done by White et al. (2012). In this analysis, $\sim 70,000$ quasars in the redshift range 2.2 to 3.4 are studied. In a more recent study, Chehade et al. (2016) combine the optical photometry of the 2dF Quasar Dark Energy Survey pilot (2QDES) and the bands of the Wide-field Infrared Survey Explorer (WISE) to provide a sample of $\sim 10,000$ QSO in the redshift range 0.8 to 2.5. Our study uses a larger and wider QSO sample than in previous works.

White et al. (2012) compute the bias of their sample, $b \sim 3.5$, which is in agreement with previous results. Using this bias, they estimate that quasars cover a wide range of halo masses between $10^{11.59} M_\odot$ and $10^{12.65} M_\odot$. These values of masses are still in agreement with our results shown in Table 3. Shen et al. (2013) found that the cross-correlation between CMASS galaxies and QSO is well modelled by a power-law, $\xi_{QG} = (r/r_0)^\gamma$, with $r_0 = 6.61 \pm 0.25 h^{-1}$ Mpc and $\gamma = 1.69 \pm 0.07$ for scales $r = 2 - 25 h^{-1}$ Mpc. Nevertheless, they had large degeneracies between their parameters. In the somewhat similar case of ELG, Favole et al. (2015) faced an equivalent problem to describe their clustering. They use constraints from lensing measurements to understand the clustering on the smallest scales. Richardson et al. (2012) predict a mean halo mass for central halos, $M_{cen} \sim 10^{12.77} M_\odot$ and Shen et al. (2013) find a characteristic mean halo mass of $10^{12.8} M_\odot$. Both HOD analysis predict halo masses which are in agreement within $1-\sigma$ errors with our measurements ($\sim 10^{12.7} M_\odot$). Richardson et al. (2012) obtain that 7.4×10^4 QSO are satellites. In contrast, a non-negligible fraction in predicted by Shen et al. (2013). They find that 6.8 per cent of QSO are hosted by sub-halos. If we do not fix the fraction of satellites, our model predicts a $\sim 5\%$ of quasar living in sub-halos, which is in a better agreement with Shen et al. (2013). However, due to the degeneracy between V_{mean} and f_{sat} , our model could also reproduce the clustering with a small fraction of satellites as is done by Richardson et al. (2012). Chehade et al. (2016) results are compared with other surveys (SDSS, 2QZ and 2SLAQ). As in previous works, they find no-evidence of a dependency between the clustering and the luminosity of the QSO. In addition, they also show that the quasar clustering depends on the redshift, in particular, when BOSS data is included. They describe the clustering of the sample by a power-law, where $r_0 = 7.3 \pm 0.1 h^{-1}$ Mpc at redshift 2.4, while the correlation scale for the whole redshift range is $r_0 = 6.1 \pm 0.1 h^{-1}$. Their measurements are consistent with host halos of mass $\sim 10^{12.46}$. Using our model, the signal of the clustering in the lin-

Table 5. Mass prediction of halos hosting quasars for different samples. It is presented name of the method used to analyse the sample and the used redshift range. ¹This work, ²Shen et al. (2013), ³Richardson et al. (2012), ⁴White et al. (2012), ⁵Eftekharzadeh et al. (2015), ⁶Chehade et al. (2016)

Sample	N_{qso}	z	Method	$\log_{10}(M_h/M_\odot)$
eBOSS ¹	68,269	0.9–2.2	HAM	12.5–12.82
SDSS-I/II ²	8198	0.3–0.9	Power-law fit	12.75
SDSS-I/II ³	48,000	0.4–2.5	HOD	12.70–12.77
BOSS ⁴	27,129	2.2–2.8	Power-law fit	12.59–11.65
BOSS ⁵	55,826	2.2–2.8	Power-law fit	11.63–12.63
2QDES ⁶	10,000	0.8–2.5	Power-law fit	12.17–12.64

ear regime is dominated by the mean halo mass of the distribution. This is clear in the halo occupation distribution (Figure 8), where the distribution has a strong peak near to the mean halo mass of the sample. We find a more constrained HOD region for quasars than Shen et al. (2013); however, it is needed more information from small scales to have better constraints in the satellite fraction and width of the distribution in order to provide more realistic uncertainties. We find a bias equal to 2.37 ± 0.12 for the redshift range $0.9 < z < 2.2$, which is in good agreement with previous analysis and with eBOSS data from Laurent et al. (in prep) (Figure 6). We provide measurements for the evolution of the bias using the BigMDPL-QSOZ light-cone, finding that the eBOSS Quasars are in agreement with $b_0 = 1.54, 2.08, 2.21, 3.15$ for redshift 1.06, 1.35, 1.65, 1.98. In addition, to give a complete parametrisation of the scales studied in this work, we calculate the second order bias from the cross-correlation coefficients, finding $b_2 = 0.314 \pm 0.030$. Table 5 presents a comparison of the halo mass prediction of previous studies and our result.

Future surveys will increase the measurements of the ELG and QSO clustering, giving the opportunity to study the cross correlation between both population, and giving information which could provide strong constraints in the parameters of our model.

6 SUMMARY

We modelled the clustering of $\sim 70,000$ optical quasars from the eBOSS Y1Q CORE sample in the redshift range $0.9 < z < 2.2$. We used a modified halo abundance matching that takes into account the incompleteness of the QSO sample and the intrinsic scatter between QSOs and dark matter halos. This model was implemented in a light-cone constructed from a $2.5 h^{-1}$ Gpc simulation, which covers an area comparable to the eBOSS Y1Q sample.

Our main results can be summarised as follows.

- We assume that the V_{max} distribution of halos hosting QSOs is described by a Gaussian function, which is defined with two parameters plus one parameter for the satellite fraction. The observations do not bear information on small scales clustering. For this reason, we cannot constrain the fraction of satellites. Hence, we do not distinguish between host and sub halos when the selection is done. The final mock thus has the same fraction of satellites as the complete simulation in the mass range used.
- The prediction of our model is in a good agreement with the 2PCF and the monopole of the power spectrum of the Y1Q data. The light-cone is constructed assuming Gaussian redshift errors given by Dawson et al. (2016). The use of these errors improve the agreement between the model and the data, providing a good

description of the small scales of the observed clustering, which is very sensitive to variations caused by those errors.

- We construct three kinds of light-cones: one including the evolution of the parameters with redshift (BigMDPL-QSOZ), the second one describing the whole redshift range with a single set of parameters (BigMDPL-QSO) and the third one fixing the satellite fraction to zero (BigMDPL-QSO-NSAT). The mean halo masses are $10^{12.61} M_{\odot}$, $10^{12.66} M_{\odot}$ and $10^{12.70} M_{\odot}$ respectively.

- Using the Bayes factor we find a strong evidence that the BigMDPL-QSOZ (4-parameters) reproduces better the data than the BigMDPL-QSO (1-parameter). However, we cannot make the same conclusion with the model without satellites, which reproduces the data with a similar agreement to the BigMDPL-QSOZ model.

- We find a mean bias of the Y1Q sample equal to 2.37 ± 0.12 and a second order bias $b_2 = 0.314 \pm 0.030$, which describe the relation between the dark matter and the QSO mock for the studied scales.

BigMDPL-QSOs and GLAM-QSO eBOSS mocks are publicly available through the *Skies and Universes* website³

REFERENCES

- Alam S., et al., 2016, preprint, ([arXiv:1607.03155](https://arxiv.org/abs/1607.03155))
 Alonso D., 2012, preprint, ([arXiv:1210.1833](https://arxiv.org/abs/1210.1833))
 Baldauf T., Smith R. E., Seljak U., Mandelbaum R., 2010, *Phys. Rev. D*, **81**, 063531
 Behroozi P. S., Conroy C., Wechsler R. H., 2010, *ApJ*, **717**, 379
 Behroozi P. S., Wechsler R. H., Wu H.-Y., 2013, *ApJ*, **762**, 109
 Berlind A. A., Weinberg D. H., 2002, *ApJ*, **575**, 587
 Bovy J., et al., 2011, *ApJ*, **729**, 141
 Bryan G. L., Norman M. L., 1998, *ApJ*, **495**, 80
 Busca N. G., et al., 2013, *A&A*, **552**, A96
 Chehade B., et al., 2016, preprint, ([arXiv:1603.04849](https://arxiv.org/abs/1603.04849))
 Cole S., et al., 2005, *MNRAS*, **362**, 505
 Conroy C., Wechsler R. H., Kravtsov A. V., 2006, *ApJ*, **647**, 201
 Cooray A., Sheth R., 2002, *Phys. Rep.*, **372**, 1
 Dawson K. S., et al., 2013, *AJ*, **145**, 10
 Dawson K. S., et al., 2016, *AJ*, **151**, 44
 Dekel A., Lahav O., 1999, *ApJ*, **520**, 24
 Delubac T., et al., 2015, *A&A*, **574**, A59
 Eftekharzadeh S., et al., 2015, *MNRAS*, **453**, 2779
 Eisenstein D. J., et al., 2005, *ApJ*, **633**, 560
 Eisenstein D. J., et al., 2011, *AJ*, **142**, 72
 Favole G., et al., 2015, preprint, ([arXiv:1507.04356](https://arxiv.org/abs/1507.04356))
 Feldman H. A., Kaiser N., Peacock J. A., 1994, *ApJ*, **426**, 23
 Font-Ribera A., et al., 2014, *J. Cosmology Astropart. Phys.*, **5**, 027
 Gunn J. E., et al., 2006, *AJ*, **131**, 2332
 Guo Q., White S., Li C., Boylan-Kolchin M., 2010, *MNRAS*, **404**, 1111
 Guo H., Zehavi I., Zheng Z., 2012, *ApJ*, **756**, 127
 Guo H., et al., 2014, *MNRAS*, **441**, 2398
 Guo H., et al., 2015, preprint, ([arXiv:1505.07861](https://arxiv.org/abs/1505.07861))
 Hahn C., Scoccimarro R., Blanton M. R., Tinker J. L., Rodriguez-Torres S., 2016, preprint, ([arXiv:1609.01714](https://arxiv.org/abs/1609.01714))
 Hartlap J., Simon P., Schneider P., 2007, *A&A*, **464**, 399
 Jing Y. P., Mo H. J., Börner G., 1998, *ApJ*, **494**, 1
 Klypin A., Yepes G., Gottlöber S., Prada F., Hess S., 2014, preprint, ([arXiv:1411.4001](https://arxiv.org/abs/1411.4001))
 Kravtsov A. V., Berlind A. A., Wechsler R. H., Klypin A. A., Gottlöber S., Allgood B., Primack J. R., 2004, *ApJ*, **609**, 35
 Myers A. D., et al., 2015, *ApJS*, **221**, 27

- Norberg P., et al., 2001, *MNRAS*, **328**, 64
 Nuza S. E., et al., 2013, *MNRAS*, **432**, 743
 Palanque-Delabrouille N., et al., 2016, *A&A*, **587**, A41
 Pâris I., et al., 2014, *A&A*, **563**, A54
 Peacock J. A., Smith R. E., 2000, *MNRAS*, **318**, 1144
 Planck Collaboration et al., 2014, *A&A*, **571**, A16
 Porciani C., Norberg P., 2006, *MNRAS*, **371**, 1824
 Rahmati A., Schaye J., Bower R. G., Crain R. A., Furlong M., Schaller M., Theuns T., 2015, *MNRAS*, **452**, 2034
 Reddick R. M., Wechsler R. H., Tinker J. L., Behroozi P. S., 2013, *ApJ*, **771**, 30
 Reid B. A., White M., 2011, *MNRAS*, **417**, 1913
 Richardson J., Zheng Z., Chatterjee S., Nagai D., Shen Y., 2012, *ApJ*, **755**, 30
 Rodriguez-Puebla A., Behroozi P., Primack J., Klypin A., Lee C., Hellinger D., 2016, preprint, ([arXiv:1602.04813](https://arxiv.org/abs/1602.04813))
 Rodríguez-Torres S. A., et al., 2016, *MNRAS*, **460**, 1173
 Ross N. P., et al., 2009, *ApJ*, **697**, 1634
 Ross A. J., et al., 2012, *MNRAS*, **424**, 564
 Schneider D. P., et al., 2010, *AJ*, **139**, 2360
 Scoccimarro R., Sheth R. K., Hui L., Jain B., 2001, *ApJ*, **546**, 20
 Shen Y., et al., 2007, *AJ*, **133**, 2222
 Shen Y., et al., 2013, *ApJ*, **778**, 98
 Sijacki D., Vogelsberger M., Genel S., Springel V., Torrey P., Snyder G. F., Nelson D., Hernquist L., 2015, *MNRAS*, **452**, 575
 Smee S. A., et al., 2013, *AJ*, **146**, 32
 Springel V., 2005, *MNRAS*, **364**, 1105
 Trujillo-Gomez S., Klypin A., Primack J., Romanowsky A. J., 2011, *ApJ*, **742**, 16
 White M., et al., 2012, *MNRAS*, **424**, 933
 Wright E. L., et al., 2010, *AJ*, **140**, 1868
 York D. G., et al., 2000, *AJ*, **120**, 1579
 Zheng Z., et al., 2005, *ApJ*, **633**, 791

This paper has been typeset from a \LaTeX file prepared by the author.

APPENDIX A: SIMULATION RESOLUTION

In order to reproduce the observed clustering of QSO or ELG samples designed for BAO measurements, we need simulations with larger volume and a higher resolution, which resolve halos of masses $\sim 10^{12.5} M_{\odot}$.

The Y1Q sample covers $\sim 1100 \text{ deg}^2$. This area is comparable to the BigMDPL-QSO light-cone; however, the halo masses needed to reproduce the clustering of the eBOSS sample are in the limit of the resolution of the simulation.

We use the $1 h^{-1} \text{ Gpc}$ MDPL simulation to quantify the effect of incompleteness in the BigMDPL light-cone. We select two snapshots from each simulation with similar redshift (Table A1). We apply the model using the parameters of Table 3. Table A1 presents a comparison between both simulations. In terms of halo mass, both mocks constructed with the different simulations provide a mean halo mass in agreement. Similar results are found in the satellite fraction.

In terms of clustering, both simulations give reasonable results with differences of the order of 3%. Figure A1 shows the difference in the monopole between both simulations, these discrepancies are reasonable for our analysis, where errors from the data are of the order of 15%.

In addition to the large errors in the data, discrepancies between both boxes seem reasonable if we notice the other sources of error.

(i) Both simulation have different initial condition, this includes error due to the cosmic variance between simulations.

(ii) The shot noise in the correlation function is larger in the MDPL simulation due to the smaller volume.

(iii) The random selection of our model is another source of error. Shaded area in Figure A1 represents the $1-\sigma$ dispersion of 15 mocks produced with different seeds.

³ <http://projects.ift.uam-csic.es/skies-universes>

Table A1. Comparison of the halo mass for mocks constructed with the BigMDPL and MDPL simulations. For comparison, all boxes from the BigMDPL simulation in the redshift range $0.9 < z < 2.2$ were used and snapshots with nearest redshift were used from the MDPL simulation

Box	z	$\log_{10}[M/M_{\odot}]$	V_{mean}	f_{sat}
MDPL	0.987	12.41	284.25	0.08
	1.425	12.54	325.95	0.07
BigMDPL	1.000	12.40	284.25	0.11
	1.445	12.55	325.95	0.07

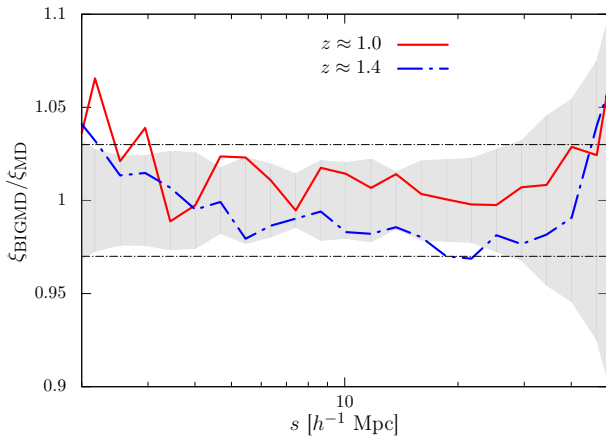


Figure A1. Ratio between BigMDPL and MDPL mocks of the monopole of the correlation function in configuration space. Horizontal lines represent 3% differences. Shaded area shows $1\text{-}\sigma$ dispersion due to the random selection in the MDPL boxes. We use 15 realisations to compute the shaded area.

(iv) The BigMDPL simulation includes long-waves which are not included in the $1\ h^{-1}\text{Gpc}$ box size.

APPENDIX B: EFFECTS OF OBSERVATIONAL ERRORS ON THE CLUSTERING

The model presented in this work includes two observational errors: Catastrophic redshift and redshift errors. The first produces a constant boost at all the scales. Figure B1 shows the effect of applying 1% of catastrophic redshifts. We find a boost of $\sim 1\%$ in all scales of the correlation function in configuration space.

Redshift errors have the strongest impact on the clustering. The selection of QSO implies fixing maximum width (precision) to identify the emission/absorption features of the spectra. We introduce the effect of this tolerance using Gaussian errors with width given by Dawson et al. (2016). Redshift errors have an important impact at scales $< 10h^{-1}\text{Mpc}$. In Figure B1, we see disagreements larger than 40%, that cannot be explained by the statistical errors of the sample (shaded area Figure B1).

The impact of redshift error is very important in the monopole of the correlation function. However, the effects of these errors in the quadrupole are very important. Figure B2 shows the ratio of quadrupole from the observed data and different mocks. The model introduced in this work describes the very large difference found between our mock and the observed data.

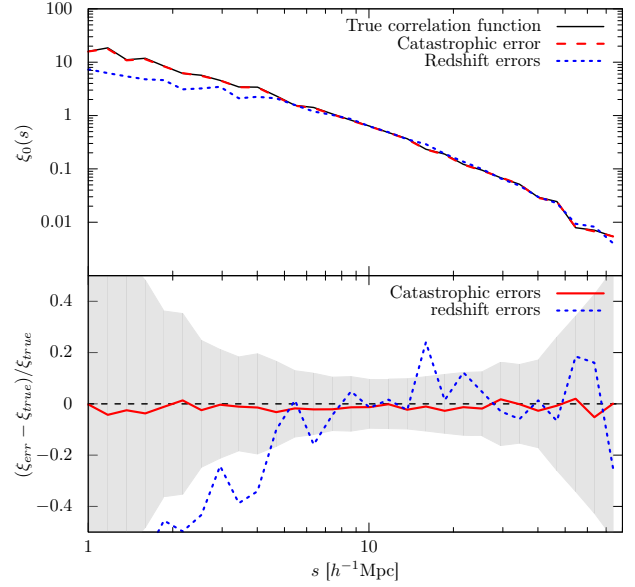


Figure B1. *Top panel:* Monopole in redshift space comparing the impact of catastrophic redshift and redshift errors. A light-cone reproducing the Y1Q 1-point and 2-point statistics is used for this comparison. *Bottom panel:* Normalised differences between mocks including redshift errors (blue dotted line) and catastrophic redshift (red solid line) with model without errors. Shaded area represent the statistical errors in the light-cone computed 1000 GLAM catalogues. Difference due to catastrophic redshift are $\sim 1\%$, while redshift error have an important impact on small scales, which cannot be explain by errors.

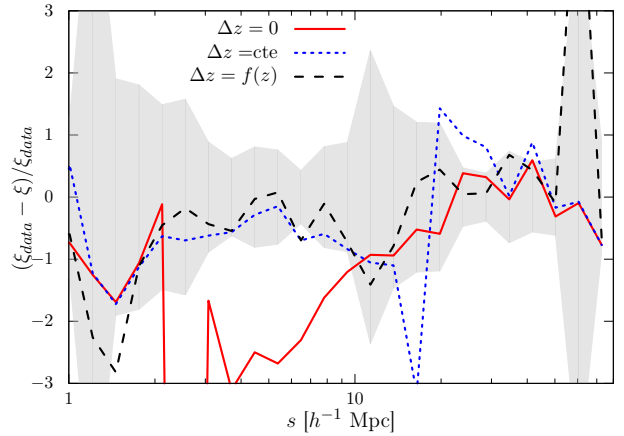


Figure B2. Impact of redshift errors in the quadrupole of the correlation function in configuration space. Lines show the normalised difference between observed data and model without redshift errors (red solid line), constant redshift error $\Delta z = 0.005$ (blue dotted line) and including redshift errors given by equation (2) (black dashed line). Shaded area represent $1\text{-}\sigma$ error computed with 1000 GLAM catalogues, for one light-cone.

ACKNOWLEDGEMENTS

SRT is grateful for support from the Campus de Excelencia Internacional UAM/CSIC.

SRT, JC, FP acknowledge support from the Spanish MICINN Consolider-Ingenio 2010 Programme under grant MultiDark CSD2009-

00064 MINECO Severo Ochoa Award SEV-2012-0249 and grant AYA2014-60641-C2-1-P.

GY acknowledges financial support from MINECO/FEDER (Spain) under research grants AYA2012-31101 and AYA2015-63810-P.

The BigMultiDark simulations have been performed on the SuperMUC supercomputer at the Leibniz-Rechenzentrum (LRZ) in Munich, using the computing resources awarded to the PRACE project number 2012060963. The authors want to thank V. Springel for providing us with the optimised version of GADGET-2.

Funding for the Sloan Digital Sky Survey IV has been provided by the Alfred P. Sloan Foundation and the Participating Institutions. SDSS-IV acknowledges support and resources from the Center for High-Performance Computing at the University of Utah. The SDSS web site is www.sdss.org.

SDSS-IV is managed by the Astrophysical Research Consortium for the Participating Institutions of the SDSS Collaboration including the Carnegie Institution for Science, Carnegie Mellon University, the Chilean Participation Group, Harvard-Smithsonian Center for Astrophysics, Instituto de Astrofísica de Canarias, The Johns Hopkins University, Kavli Institute for the Physics and Mathematics of the Universe (IPMU) / University of Tokyo, Lawrence Berkeley National Laboratory, Leibniz Institut für Astrophysik Potsdam (AIP), Max-Planck-Institut für Astrophysik (MPA Garching), Max-Planck-Institut für Extraterrestrische Physik (MPE), Max-Planck-Institut für Astronomie (MPIA Heidelberg), National Astronomical Observatory of China, New Mexico State University, New York University, University of Notre Dame, Observatório Nacional do Brasil, The Ohio State University, Pennsylvania State University, Shanghai Astronomical Observatory, United Kingdom Participation Group, Universidad Nacional Autónoma de México, University of Arizona, University of Colorado Boulder, University of Portsmouth, University of Utah, University of Washington, University of Wisconsin, Vanderbilt University, and Yale University.